

Systematics in the invariant mass analysis of D^{*+} mesons in $\sqrt{s_{NN}} = 2.76$ TeV ^{208}Pb - ^{208}Pb collisions in ALICE

Joris Ketelaars

Utrecht University, Institute for Subatomic Physics

Student ID: 3773183

Supervisors: André Mischke, Allesandro Grelli and Annelies Veen

Abstract

Using a multidimensional approach, we provide better systematic uncertainties in the analysis of the D^{*+} meson in the $D^{*+} \rightarrow D^0 + \pi_s^+ \rightarrow K^- + \pi^+ + \pi_s^+$ decay channel. This method automates a lengthy process that used to be done by hand and also gives a new method to observe the stability of fits to invariant mass plots.

Contents

1	Introduction	3
1.1	Theoretical background	3
1.2	Motivation	4
2	ALICE	6
2.1	Subdetectors in ALICE	6
2.2	Software environment	8
3	Methods	10
3.1	Particle reconstruction	10
3.2	Selection cuts	10
3.3	Multidimensional analysis on invariant mass plots	12
3.4	Automatisation of fitting	13
3.5	Processing results	14
3.6	Stability of fits	15
4	Results	16
4.1	Mean and sigma	16
4.2	Yield extraction	17
4.3	Stability of results	17
5	Conclusions	18
6	Appendix	20

1 Introduction

The goal of this thesis is to demonstrate an improved method to determine systematic uncertainties in the invariant mass analysis of D^{*+} mesons in ALICE. This method is not limited to being used specifically for D^{*+} analysis, and can also be adapted for analysis of invariant mass analysis of other particles.

1.1 Theoretical background

Particle physics is the area of physics that describes elementary particles and the interactions between them. Currently, the Standard Model is the most accurate representation of physics on that scale. It describes three groups of particles: quarks, leptons and gauge bosons. It also describes three elementary forces: the electromagnetic force, the weak force and the strong force. The strong force, described by Quantum Chromodynamics (QCD), is the most relevant one for this thesis.

QCD describes the force, mediated by gluons, that is experienced between particles with a colorcharge. Particles with a colorcharge in the Standard Model are quarks and also the gluons themselves. The fact that gluons also experience the strong force is something that makes the strong force different from the other forces in the Standard Model. An effect of this is that the strong force is mathematically difficult to describe. While going deeper into the theory of QCD is not within the scope of this thesis, there are some fundamental parts that need to be explained.

A particle with colorcharge can assume one of three types, named red, green and blue. Their antiparticles similarly assume anticolors, respectively named anti-red, anti-green and anti-blue. The combination of the three different types gives a neutral colorcharge, and the combination of a certain colorcharge with its anti-colorcharge also gives a neutral colorcharge. One of the properties of QCD is confinement, which states that it is only possible to observe particles with a neutral colorcharge. This is due to the fact that when you try to separate two quarks, the energy needed is so large that it becomes more energy efficient to create a quark-antiquark pair to fill the gap than to leave it empty. Since we can only observe colorless particles, the hadrons that can be observed are either quark-antiquark pairs, or threesomes of either quarks or anti-quarks.

Another related property of QCD is asymptotic freedom. While the

strong force becomes stronger as you try to separate quarks, when the distance between two quarks decreases, the strong force weakens. Because of this, we expect a different state of matter to occur when the particle-density increases. When hadrons are forced close enough together, quarks and gluons start interacting freely and are no longer confined by the boundaries of the hadrons they were part of. We call this state the Quark Gluon Plasma (QGP). One of the goals of the LHC project, and recent particle physics in general, is to observe a QGP.

Since we cannot observe the particles in the QGP directly, we use an alternative method to measure a QGP. When the QGP expands and cools down, the quarks in it condense into hadrons, which can be observed. These hadrons then leave the QGP in hadronic jets, the properties of which can tell us something about the QGP.

1.2 Motivation

More precisely we compare D^{*+} mesons in ^{208}Pb - ^{208}Pb and p-p collisions. In the latter we have just 2 protons colliding, while the lead-atoms that are used have 82 protons, and 126 neutrons. The increased density in Pb-Pb collisions means that a QGP might occur, but because of its short lifetime (10^{-23}s), we cannot measure it directly. Instead, we use probes, particles flying away from the collision to tell us something about the short-lived medium it came from. Because the major force at work in that medium is the strong force, we cannot use leptons, because they don't experience this force. Quarks and gluons we cannot measure independently, so we need to look at hadrons.

We prefer to look at hadrons containing heavier quarks because the light quarks have a higher chance of being absorbed into the medium. The heavy quarks also experience less energy losses due to gluon radiation because of the dead-cone effect, which means that the interaction with the medium plays a relatively larger role, which is exactly what we are interested in.

Since the top-quark decays so fast that it does not condense into a hadron, we need to look at hadrons containing charm- or beauty-quarks. These can bond with their antiparticles to create quarkonium particles (such as the J/Ψ), or with a lighter quark, to create B- or D-mesons. The D^{*+} is so short-lived, that it decays before reaching the innermost subdetector in ALICE, so we need to look at the decay products and reconstruct them. Because of this, we like to look at purely hadronic decay-channels. The most prominent of these for our D^{*+} is $D^{*+} \rightarrow D^0 + \pi_s^+$ with a branching ratio of $67.7 \pm 0.5\%$. [4]

With the D^0 then decaying to $D^0 \rightarrow K^- + \pi^+$ with a branching ratio of $3.88 \pm 0.05\%$. [5]

This low branching ratio, combined with the relatively rare production of heavy quarks, means that we get a low yield. Compared to p-p collisions, we also have a lot more background, because a lot more particles are generated for every event. Together, they make the analysis of data difficult.

After selection cuts are made for potential D^{*+} 's, a fit is made to invariant mass plots, from which results such as the yield can be extracted. The analysis of invariant mass plots used to be done by hand, which was a time-intensive and error-sensitive task. Automatisation of this process not only makes it easier, but also provides new insights in the analysis of the data.

2 ALICE

ALICE (an abbreviation for A Large Ion Collider Experiment) is one of the major detectors used at the LHC (Large Hadron Collider) at CERN.[1] It was specially build to study high multiplicity collisions, such as Pb-Pb ones, but it is also capable of performing measurements in p-p collision. This is useful in providing a comparison, since the same detector can be used for both cases.

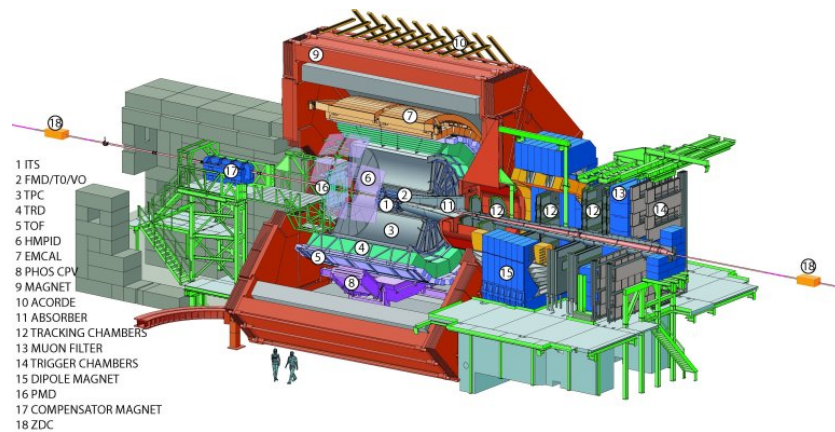


Figure 1: A sketch outlining the different components of ALICE.

2.1 Subdetectors in ALICE

The particles we reconstruct are short lived, so the main detectors used to take the data used by this thesis are the inner ones. The inner ones are situated in the Central Barrel inside a 0.5 Tesla magnet that has carried over from the earlier LEP experiment that used to be situated where the LHC now is. While discussing the whole ALICE detector and its components are outside the scope of this thesis, we would like to highlight the ones important for the measurement of D-mesons.

The T0 and V0 triggers are Cherenkov detectors that are used as a trigger to determine with as much precision as possible when the event took place, it does this with a resolution of about 10^{-10} seconds.

The ITS is the inner tracking system, it consists of 6 layers that use 3 different types of silicon detectors. The ITS can track high (higher than

1 GeV/c) momentum particles with very high precision. (Measuring with a resolution better than 1 millimeter.) It can also track particles with momenta of less than 100 MeV/c, which makes it unique in all the detectors of ALICE, and also crucial, since it is the only detector that can detect the π_s^+ daughter products in our decay channel. Particle identification (PID) is done in the ITS by measuring energy losses, which can be seen in figure 2.

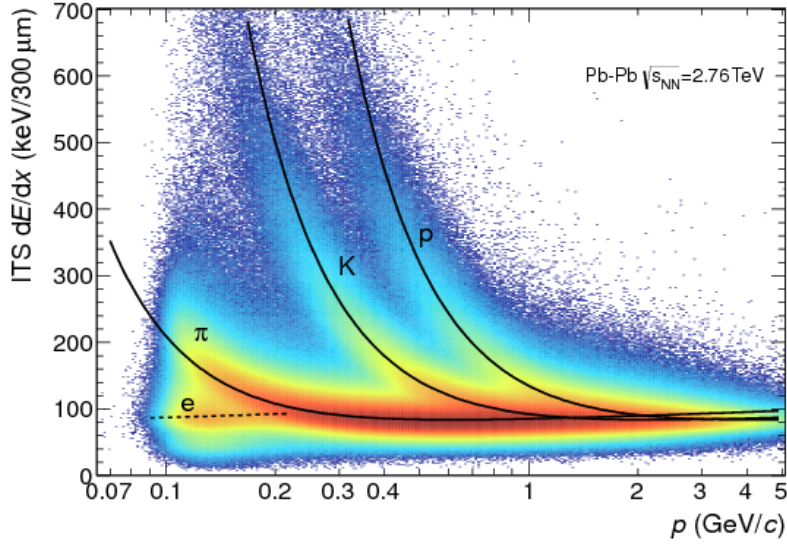


Figure 2: Energylosses in the ITS as a function of particle energy, distinction between different particles is easiest for low energy particles.

The time projection chamber (TPC) is the main detector used for tracking particles in ALICE, it is an electrostatically-charged gas-filled chamber. The cylinder shaped chamber is situated around the other inner detectors. Whenever a particle travels through the TPC, it ionizes a trail and liberated electrons drift through the chamber towards the end plates where wire chambers are situated that measure these electrons. The TPC gives the energy loss of a particle, as well as the precise path it has travelled. Together with the ITS and TOF detectors next to it, it is responsible for generating enough hits to allow the reconstructing of tracks.

The time of flight detector (TOF) is a gas chamber filled with plates which is used to time the arrival time of incoming particles. Combined with the T0 and V0 triggers, a time of flight can be calculated, which together

with the momentum can be used to calculate the mass of a particle, and use this to identify particles.

2.2 Software environment

The software packages used for this thesis are ROOT and AliRoot.

ROOT is a C++ package that was made to perform particle physics research. It contains many premade packages that can perform event simulations, data analysis and visualize results. AliRoot is an extension focused on the ALICE detector, and the many research group that work with this detector.[6] The D^{*+} analysis was done using code from the VertexingHF folder inside the PWGHF folder. (Particle Work Group Heavy Flavour). Specifically a slightly modified version of the *AliMassFitter.cxx* file was used to perform the fitting, and a new macro *VariableFitMass.C* based on the *FitMassSpectraJ.C* was used to perform the multidimensional analysis.

The *AliMassFitter.cxx* fits to invariant mass plots in several steps. First it performs a background fit using only background data by not taking into account any bins in a region around your expected Gaussian. Results from this fit are then used as a starting point to perform a complete fit using the full set of bins, and using function4. Fitting is done using the MINUIT process. The MINUIT process can give runaway solutions as minimal ones, which is why the *AliMassFitter.cxx* was changed. Without limiting solutions, the macro is inclined to give floating point errors when a runaway solution is found. Using limitations on your solutions gives a much more stable code that is less likely to crash than the *AliMassFitter.cxx* that is included by default in the ALICE package. Results from the fitting process look like figure ??.

The *VariableFitMass.C* splits your data in several (9 used here, for comparison with the results from p-p collisions) pt-bins, and performs in a loop to analyze each pt-bin separately. Each time it works in three nested loops that are used to vary 3 parameters of your analysis process (first used bin, re-binning value, and maximum range). Every increment, starting values from a Monte Carlo simulation are send to the *AliMassFitter.cxx* function to make sure the fitter is capable of finding a fit. The code is also capable of fixing the mean and/or sigma of your fit. The *AliMassFitter.cxx* function is then called to perform a fit to your invariant mass data, and results are stored in arrays. After the looping process is done, which takes around 5 minutes on a modern laptop, the results are stored in a TFile, drawn as TGraphs and

results are shown for each pt-bin in histograms.

The code was ran on the authors laptop, running 64-bit Ubuntu, using the CINT interpreter.

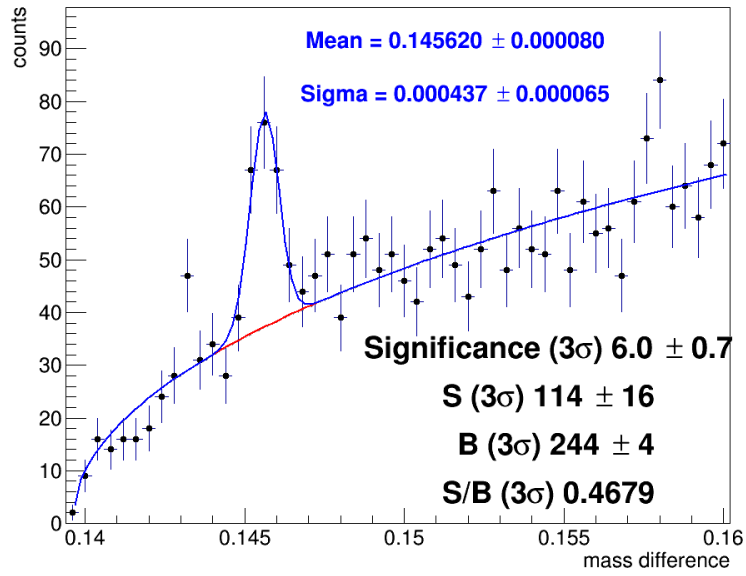


Figure 3: A fit to the invariant mass data for 6-8 GeV/c pt-bin. 5

3 Methods

The detectors in ALICE generate electrical signals whenever particle enters them. Reconstructing tracks from these electrical signals is a complicated process that is done centrally at CERN. After that is done, we have a list of events that consist of multiple tracks. We would like see the events and tracks that involve a D^{*+} , this is however not directly possible, because the D^{*+} decays so fast that it does not reach the innermost detector inside ALICE.

Whenever the D^{*+} is mentioned in this thesis, its antiparticle D^{*-} is also taken into account.

3.1 Particle reconstruction

For the decay-channel $D^{*+} \rightarrow D^0 + \pi_s^+ \rightarrow K^- + \pi^+ + \pi_s^+$, we need to reconstruct the D^{*+} from 3 particles. This is because the D^0 also decays before the innermost detector, so it too cannot be directly measured. It can however be reconstructed from its two daughter particles, and since it is neutral, we can assume it came straight from the collision. The sum of the energies of these two daughter particles also needs to be larger than the mass of the D^0 (1864.80 ± 0.17 MeV/ c^2)[5], because they cannot come from a D^0 if that is not the case.

Because there are many other decay-channels, and the rarity of the D^{*+} in the first place, almost all tracks you have are just background. In order to select potential D^{*+} mesons, you need to apply physical cuts. These need to be strict enough so that you get rid of as much background as possible. But you cannot make them too strict, because there are also fluctuations in the tracks that come from the D^{*+} , because of uncertainties in the detectors for example.

3.2 Selection cuts

The following cuts are applied to the data to filter out background amongst your D^{*+} -candidates, which is done to filter away background. Choosing cuts is a balancing act between cutting away as much background as possible while retaining most of your D^{*+} . The process of making selection cuts is something that also influences the systematic uncertainties, but incorporating that into this process was outside of the scope of this work. We will

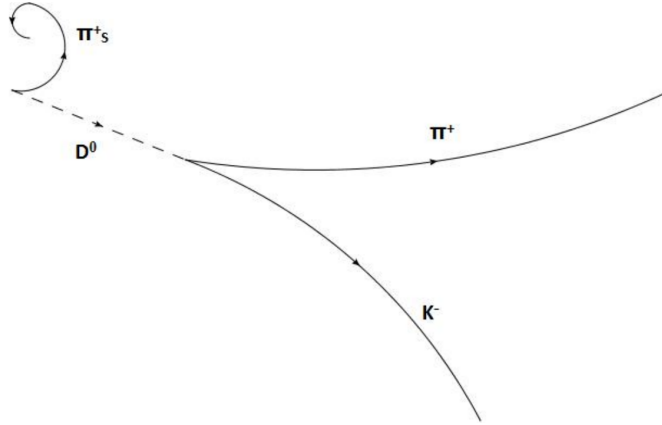


Figure 4: Sketch of the hadronic decay: $D^{*+} \rightarrow D^0 + \pi_s^+ \rightarrow K^- + \pi^+ + \pi_s^+$.

list the selection cuts that are being done, but for more details, we would like to refer to one of our supervisors.[2]

- Invariant mass window for the D^0 .
- The distance of closest approach between the K^- and the π^+ .
- The cosine of the angle between the reconstructed D^0 and K^- .
- The transverse momentum of the π_s^+ , π^+ and K^- .
- The impact parameter of the π^+ and K^- .
- The product of the impact parameters of π^+ and K^- .
- The cosine of the pointing angle.
- The deviation of the reconstructed D^{*+} from its PDG-value.
- The deviation between the massdifference between the reconstructed D^{*+} and the D^0 and the expected value from the PDG-values.
- The cosine of the angle between the π_s^+ and the reconstructed D^0

3.3 Multidimensional analysis on invariant mass plots

In order to make a better comparison with the results from the p-p collisions, the data is split up into 9 pt-Bins: 2-3 GeV/c, 3-4 GeV/c, 4-5 GeV/c, 5-6 GeV/c, 6-8 GeV/c, 8-12 GeV/c, 12-16 GeV/c, 16-24 GeV/c, 24-36 GeV/c.

In order to observe our D^{*+} , we look at the mass difference between potential D^{*+} and the D^0 .

$$\Delta m = m_{D^{*+}} - m_{D^0} \quad (1)$$

The minimum of this value is the mass of a π^+ , because the decay cannot happen if this mass were smaller. When the mass difference is put in a histogram, we can then extract information from it by applying a fit. The invariant mass can look like the one in figure 5 for example. Since the data is a combination of background and decays from the D^{*+} , we fit the sum of two functions that describe them individually. For the D^{*+} decay product we expect a simple Gaussian,

$$f(\Delta m) = \frac{yield}{\sqrt{2}\sigma} e^{-0.5(\frac{\Delta m - \mu}{\sigma})^2} \quad (2)$$

where *yield* is the surface area of the gaussian and therefore our total number of measured D^{*+} . μ is the mean, and σ is the standard deviation of our gaussian. For the background we use

$$f(\Delta m) = a\sqrt{\Delta m - m_\pi} e^{b(x - m_\pi)} \quad (3)$$

where a and b are variables that define the background, and m_π the mass of the pion. The sum of the two becomes the function to which we fit our invariant mass histograms.

$$f(\Delta m) = a\sqrt{\Delta m - m_\pi} e^{b(\Delta m - m_\pi)} + \frac{yield}{\sqrt{2}\sigma} e^{-0.5(\frac{\Delta m - \mu}{\sigma})^2} \quad (4)$$

Before the fitting process can be performed, some extra parameters need to be chosen. Whilst the minimum range is quite obvious, namely the mass of a π^+ , m_π , the maximum range can be chosen somewhat freely. The maximum range needs to be high enough so that there are enough datapoints to make a background-only fit. The maximum range also cannot be chosen higher than 170 MeV/c, because the data is not reliable above this value. You also need

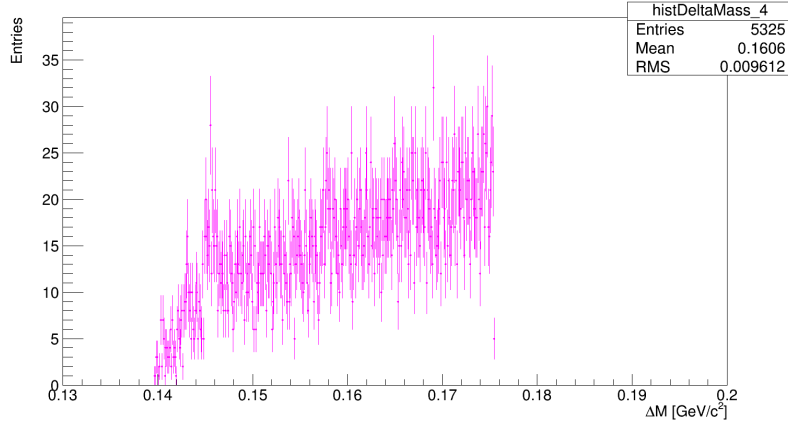


Figure 5: Δm distribution after selection cuts are applied, for the 6-8 GeV pt-bin.

to rebin your histogram, combine several bins into one. This lowers both the uncertainties in the individual bins and decreases the spread amongst them in total. Ideally you would want a high rebin value that leaves you with enough points to make a decent fit. Which means it must be low enough so that you still have several (4-5) bins in the region where you find your Gaussian.

Grouping bins together gives different results depending on where you start counting bins, since discarding one or more of the first bins changes what bins are used to regroup. Overall, we have to choose three variables: maximum range, rebin value and the first used bin. After that is done, a fit can be made.

3.4 Automatisations of fitting

Determining what values to chose for these parameters used to be done by hand, since choosing them at random has a significant influence on the quality of your fit, sometimes a fit might not even be found because of low statistics. Even after picking only good fits with a decent χ_{red}^2 value and a high significance, you end up with results that can fluctuate. Instead of manually looking for best fits, new code was written that varies the following variables.

- The maximum range was varied using results from a Monte-Carlo sim-

ulation as a baseline. With μ and σ the mean and sigma from the MC simulation, we fluctuated the maximum range between $\mu + 10\sigma$ and $\mu + 25\sigma$. The maximum range was incremented by 1 bin at a time, to make sure that every histogram fitted was unique.

- The amount of bins combined into new bins was varied between 2 and 10.
- The first used bin for the process was varied between 1 and 5, although the first used bin was kept smaller than the amount of rebins. This was done because the removal of the first bin in your rebinned histogram has a minimal effect.

3.5 Processing results

The above variables were fluctuated in a loop, with a fit being applied after every incrementation. A selection was then made on the fit in order to exclude bad fits. Fits that did not have $0.9 < \chi_{red}^2 < 1.1$ were excluded, aswell as fits that returned values for the mean or sigma that deviated significantly from the results from the MC simulation. (If the MC mean and sigma lied outside of the one- σ range given by the fitter.)

After selecting fits in that way, results were stored. These included the yield, the χ_{red}^2 , the mean and the sigma of your results. An option to draw individual fits was decided against because of the amount of fits done, although a selection could be drawn trough a seperate function that allowed for visual inspection of fits.

Results were then drawn to visuallize results, aswell as written to a seperate file for easier storage and potential processing. In the ideal case, the fluctation of your results are distributed randomly around a certain value. Compared to an individual fit, the average values of these results are a more decent result for the yield, χ_{red}^2 , mean and sigma of your histogram. The spread of these results is a more decent result for the systematic uncertainty for the properties of your histogram.

In the end, we use the mean value of our values as the mean value of our parameter. The RMS of these values is a good result for the systematic uncertainty due the analysis of our invariant mass distributions.

3.6 Stability of fits

Ideally, the results found fluctuate obeying some normal distribution. This is not always the case due to low statistics. It is possible to find multiple solutions which seem stable, your results look like a sum of two disjoint Gaussian distributions. The sigma of the 12-16 GeV/c pt-bin in figure 18 is the most clear example of this. Because of this, manual inspection is needed to make sure that the reported results are reliable.

4 Results

4.1 Mean and sigma

Extracting the values from the histograms (which are found in the appendix (section6)), we get the following results for the mean in table 1 and the sigmas in table 2. While these results seem conclusive, some pt-bins are not shaped like a gaussian, but rather a convolution of 2 Gaussians. This is most clear in the 12-16 GeV/c pt-bin (figure 18), but also to a lesser extent in the 4-5 GeV/c pt-bin. (figure 10) The other pt-bins

pt-bin (GeV/c)	mean (GeV/c ²)	RMS mean (GeV/c ²)
2-3	0.14561	0.00008
3-4	0.14571	0.00006
4-5	0.14568	0.00007
5-6	0.14527	0.00004
6-8	0.14564	0.00003
8-12	0.14544	0.00008
12-16	0.14572	0.00008
16-24	0.145999	0.000002
24-36	0.14548	0.00010

Table 1: Average values and RMS of the means for every pt-bin

pt-bin (GeV/c)	sigma (GeV/c ²)	RMS sigma (GeV/c ²)
2-3	0.00039	0.00009
3-4	0.00052	0.00007
4-5	0.00055	0.00006
5-6	0.00067	0.00002
6-8	0.00050	0.00003
8-12	0.00058	0.00004
12-16	0.00087	0.00011
16-24	0.00057	0.00003
24-36	0.00097	0.00005

Table 2: Average values and RMS of the sigmas for every pt-bin

4.2 Yield extraction

For the yield, we get the following results when looking at all the returned values.

pt-bin (GeV/c)	Mean value	RMS
2-3	110	12
3-4	163	10
4-5	118	7
5-6	69	1
6-8	115	3
8-12	98	3
12-16	44	2
16-24	18	1
24-36	15	1

4.3 Stability of results

While most pt-bins behave as expected (The yield from the 6-8 GeV/c pt-bin in figure 15 is a good example.), there are some that display some pattern dependant on the maximum range.

Looking at the yield of the 4-5 GeV/c pt-bin in figure 11 we can see two clearly distinct horizontal lines. These indicate two separate stable solutions to your invariant mass analysis. The results for the sigma in the 12-16 GeV/c pt-bin also indicate two separate stable solutions, although the yield and mean seem to give the same results for this pt-bin. 18

We can see for example in the 3-4 GeV/c pt-bin in figure 9 that the yield lowers as you increase the maximum range up to 152 MeV/c, after which it is stable with respect to the maximum range. This is likely an artifact of low statistics, with one bin in this region being high enough to influence the entire results. But it could also possibly be an indication that the function (function ??) for which you fit might need a minor addition.

5 Conclusions

Choosing different parameters for your rebinning process can have a big effect on your results. Finding good parameters in the first place took a lot of time and effort. Automating this process lets the computer do this for us much more efficiently. The process still requires the human-in-the-loop though, in the beginning to set parameters so that the code knows where to look for fits. And in the end, when the human needs to distinguish that some pt-bins have multiple solutions that seem stable, and either a correct one needs to be chosen, or other course of action is needed.

Ideally the selection cuts would also perform a similar process, but the computing power needed to vary that many variables means that it is not currently possible. (Every added variable multiplies the computing time by the range over which you vary it.) But the invariant mass analysis could be more integrated with the selection cuts, to automate this process more as well. The infrastructure to perform large scale computing on the GRID is already present.

References

- [1] *A Large Ion Collider Experiment*, <http://aliceinfo.cern.ch/Public/Welcome.html>
- [2] Annelies Veen, *D^{*+} reconstruction in proton-proton interactions at $\sqrt{s} = 8$ TeV with the ALICE detector at the Large Hadron Collider*, 2014, <http://www.staff.science.uu.nl/misch101/BONZ/Thesis>
- [3] Piotr Kukla, *D^{*+} analysis in proto-proton collisions at $\sqrt{s} = 2.76$ TeV using the ALICE detector at CERN*, 2011
- [4] Particle Data Group, *$D^*(2010)^\pm$* , 2008, <http://pdg.lbl.gov/2008/listings/m062.pdf>
- [5] Particle Data Group, *D^0* , 2008, <http://pdg.lbl.gov/2008/listings/s032.pdf>
- [6] *ROOT Data Analysis Framework*, 2008, <https://root.cern.ch/drupal/>

6 Appendix

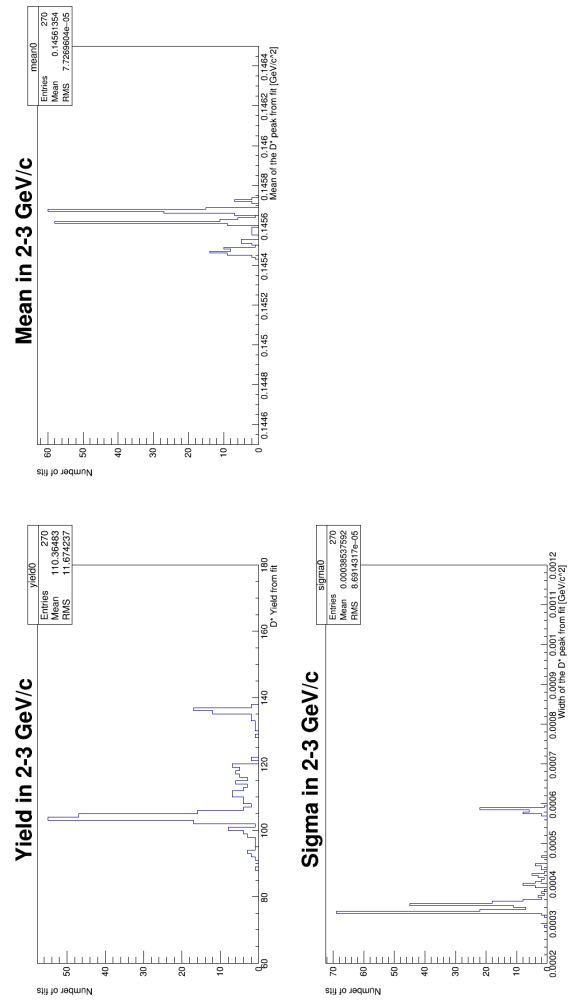


Figure 6: The yield, mean and sigma for the 2-3 GeV pt-bin.

yield 2-3 GeV/c

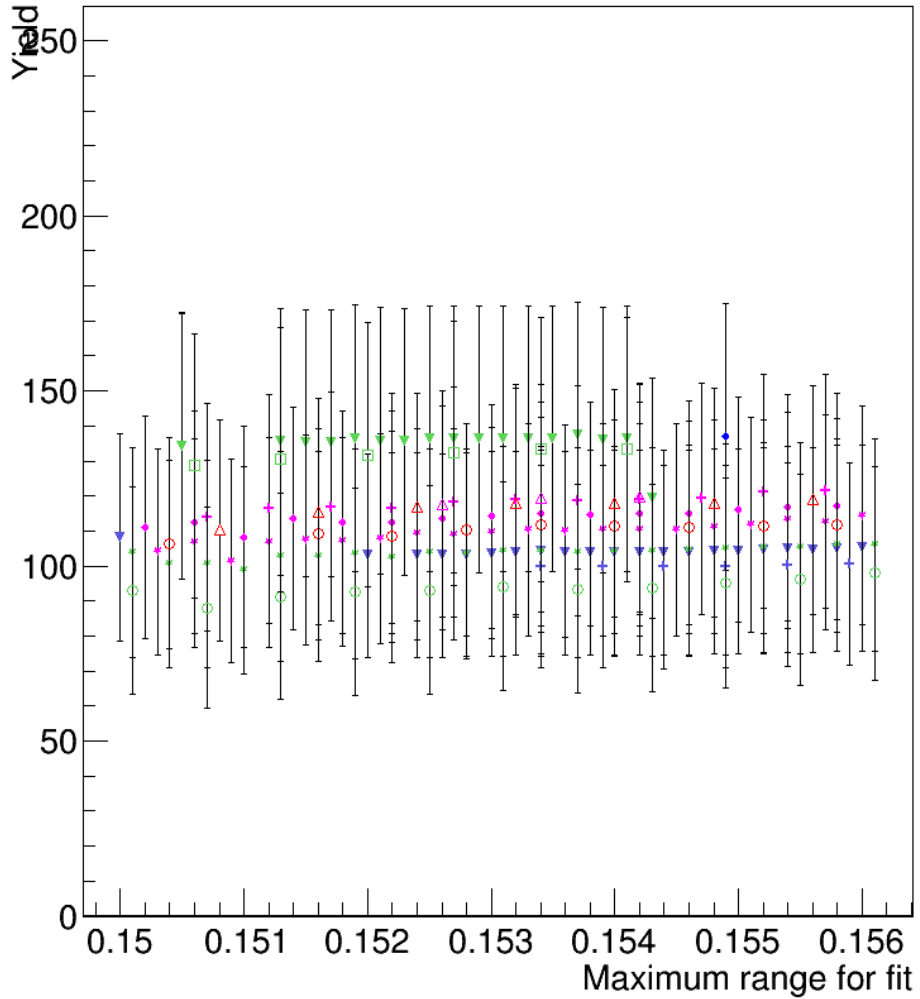


Figure 7: The yields given by fits as a function of the maximum range, points with the same color have the same first used bin, points with the same marker have the same rebinvalue.

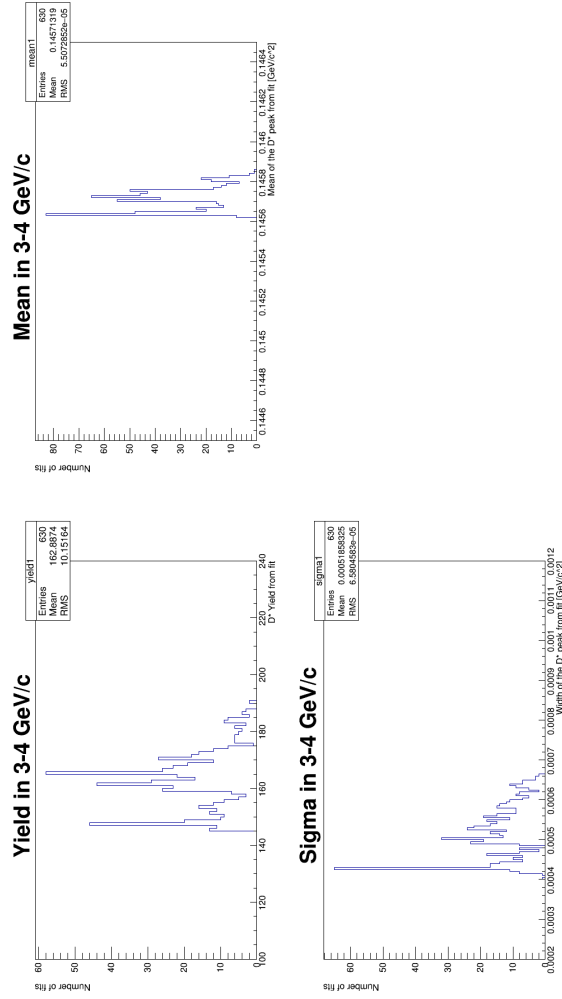


Figure 8: The yield, mean and sigma for the 3-4 GeV pt-bin.

yield 3-4 GeV/c

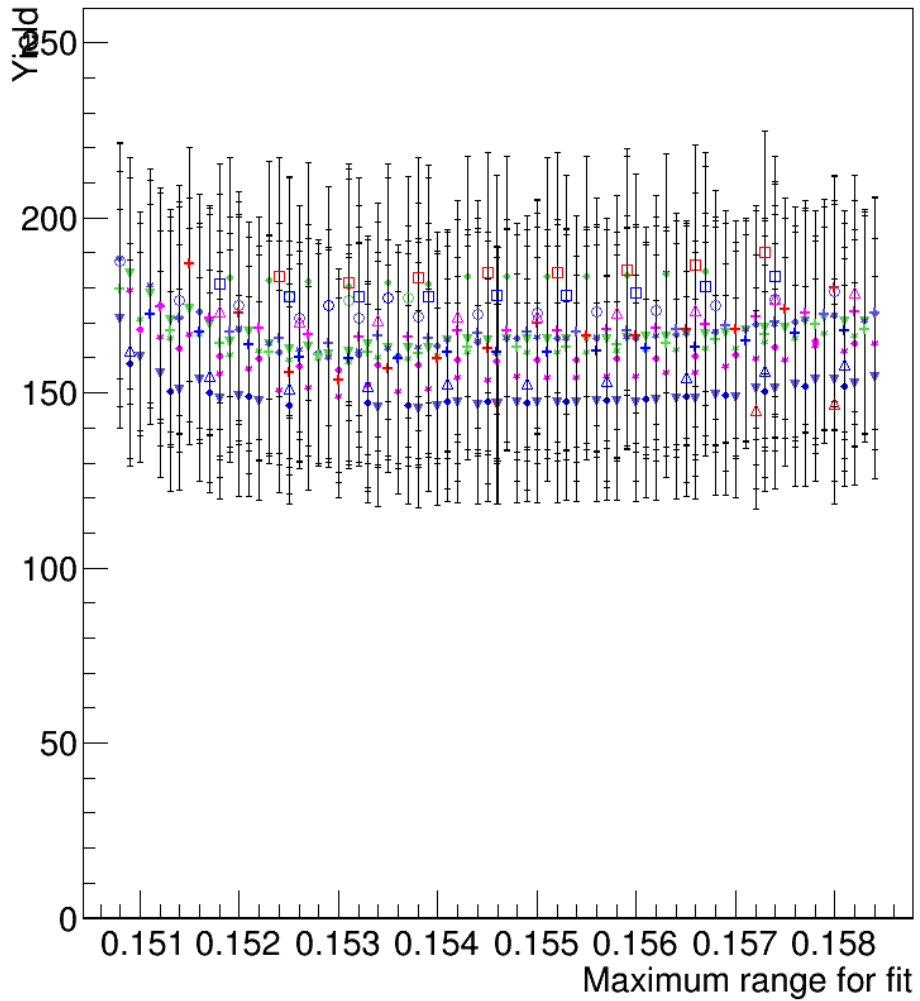


Figure 9: The yields given by fits as a function of the maximum range, points with the same color have the same first used bin, points with the same marker have the same rebinvalue.

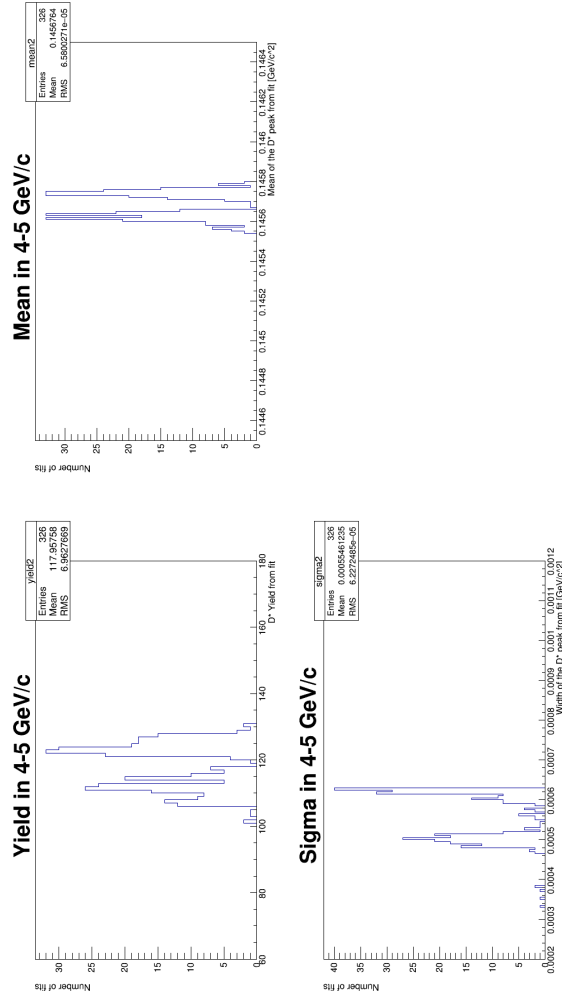


Figure 10: The yield, mean and sigma for the 4-5 GeV pt-bin.

yield 4-5 GeV/c

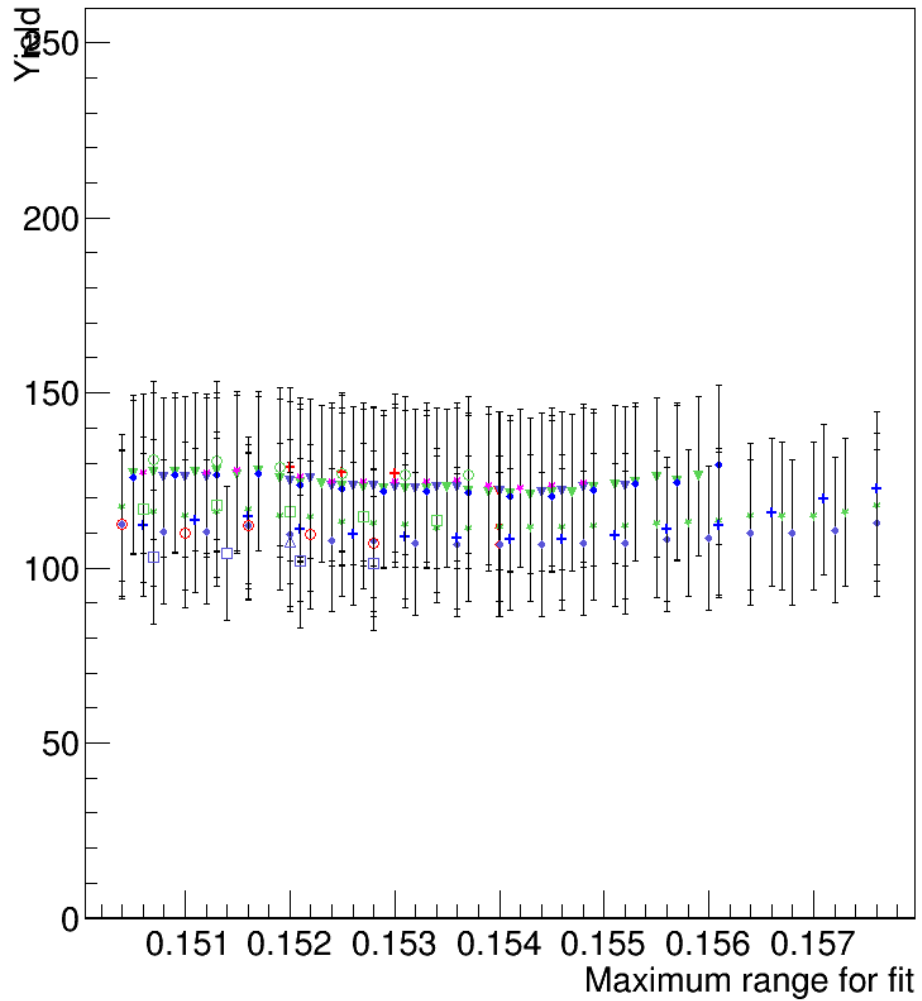


Figure 11: The yields given by fits as a function of the maximum range, points with the same color have the same first used bin, points with the same marker have the same rebinvalue.

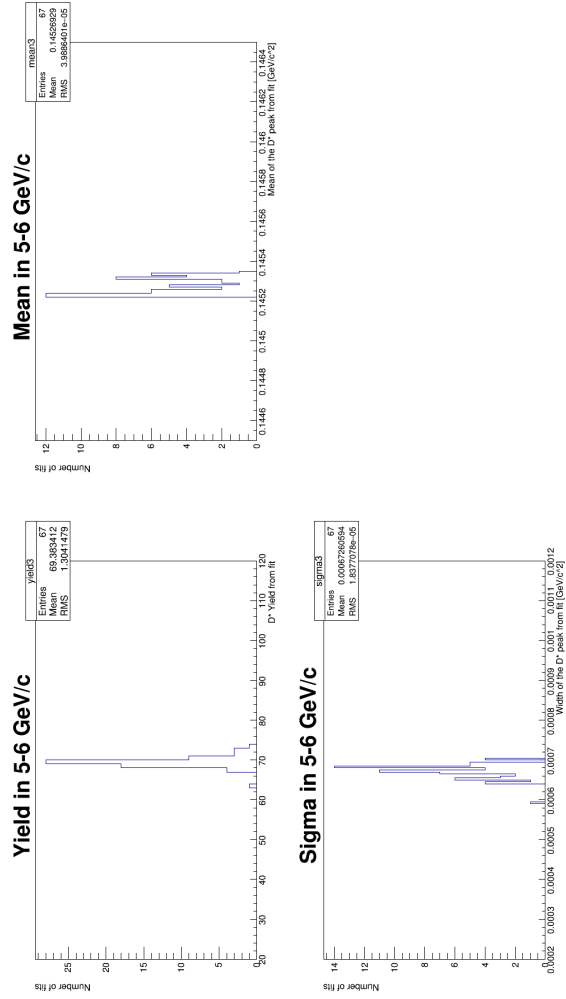


Figure 12: The yield, mean and sigma for the 5-6 GeV pt-bin.

yield 5-6 GeV/c

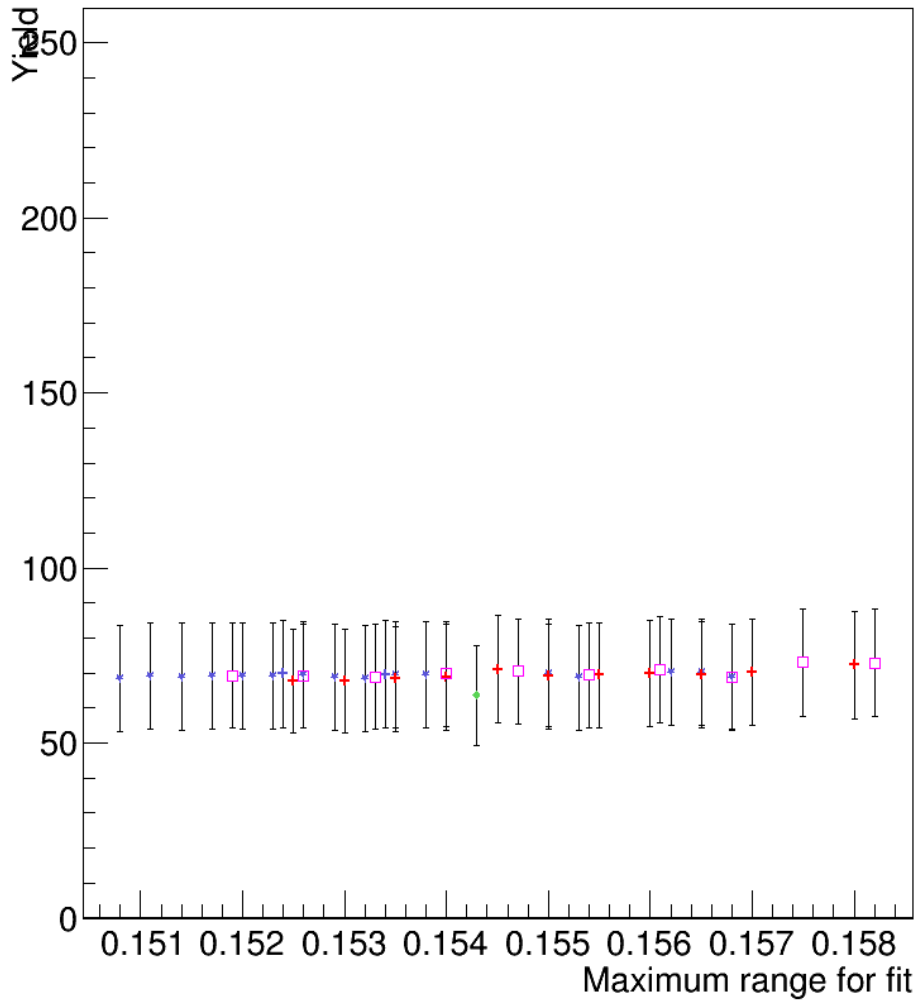


Figure 13: The yields given by fits as a function of the maximum range, points with the same color have the same first used bin, points with the same marker have the same rebinvalue.

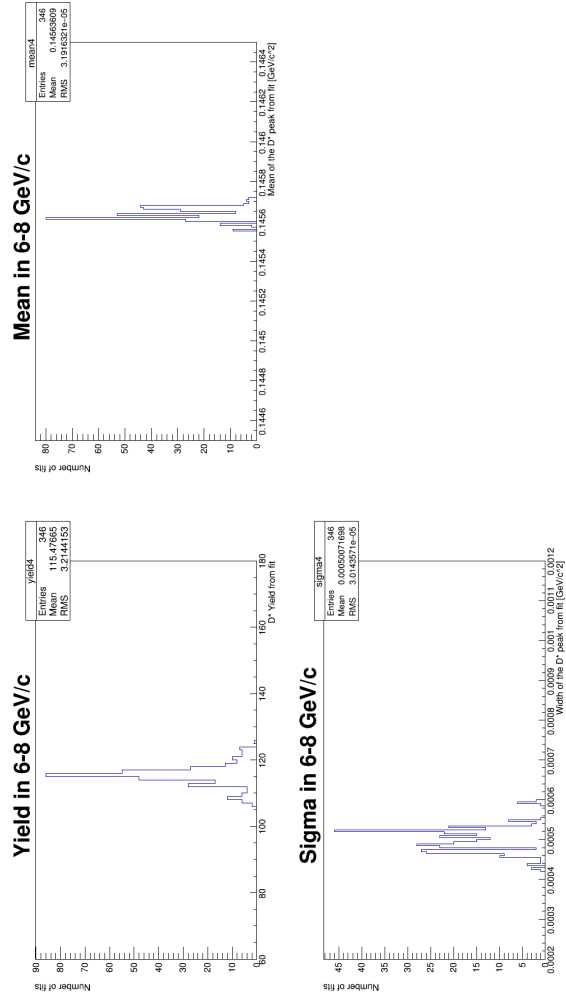


Figure 14: The yield, mean and sigma for the 6-8 GeV pt-bin.

yield 6-8 GeV/c

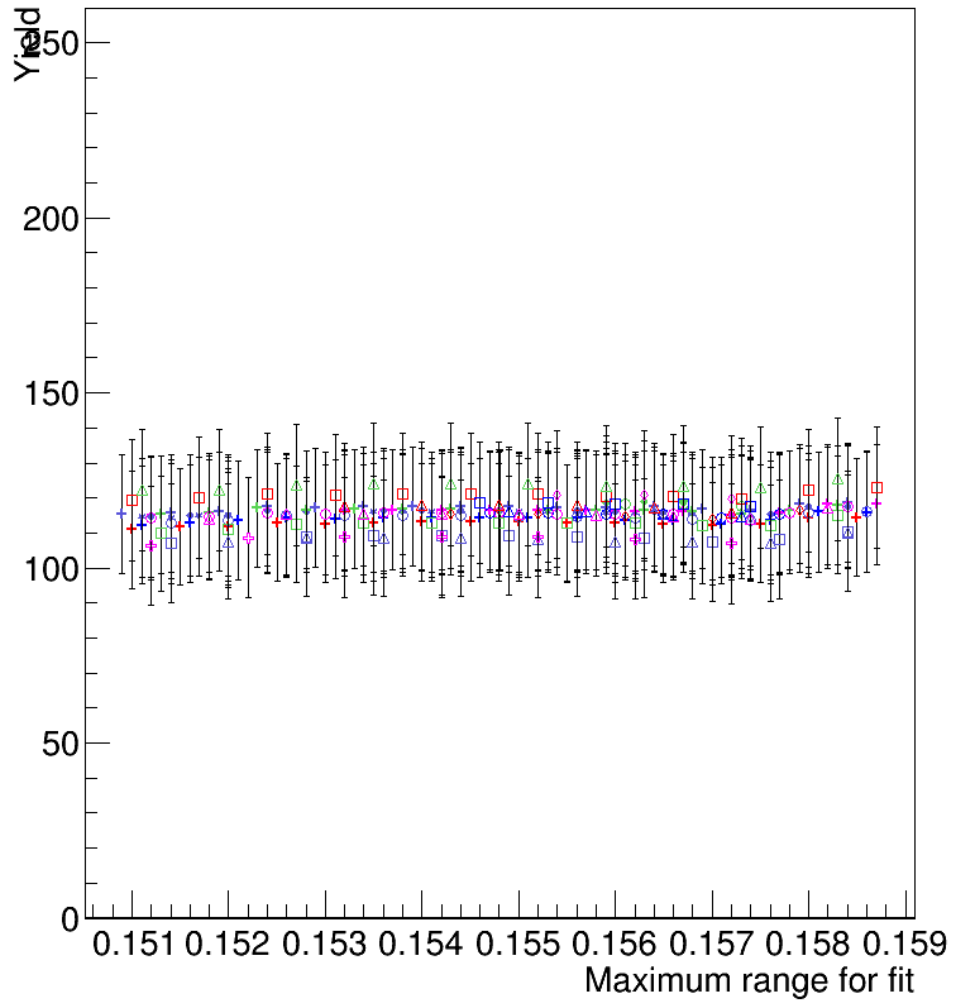


Figure 15: The yields given by fits as a function of the maximum range, points with the same color have the same first used bin, points with the same marker have the same rebinvalue.

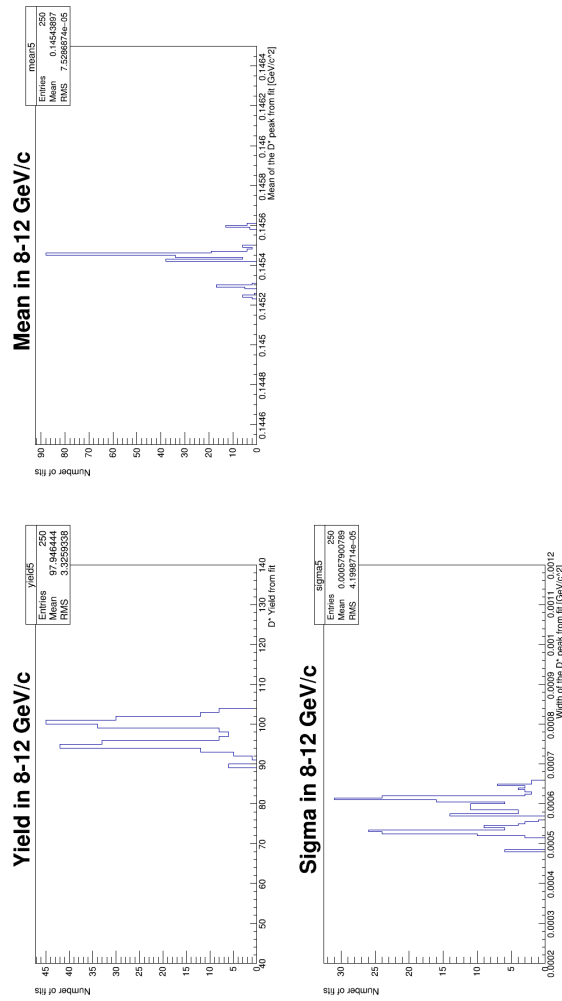


Figure 16: The yield, mean and sigma for the 8-12 GeV pt-bin.

yield 8-12 GeV/c

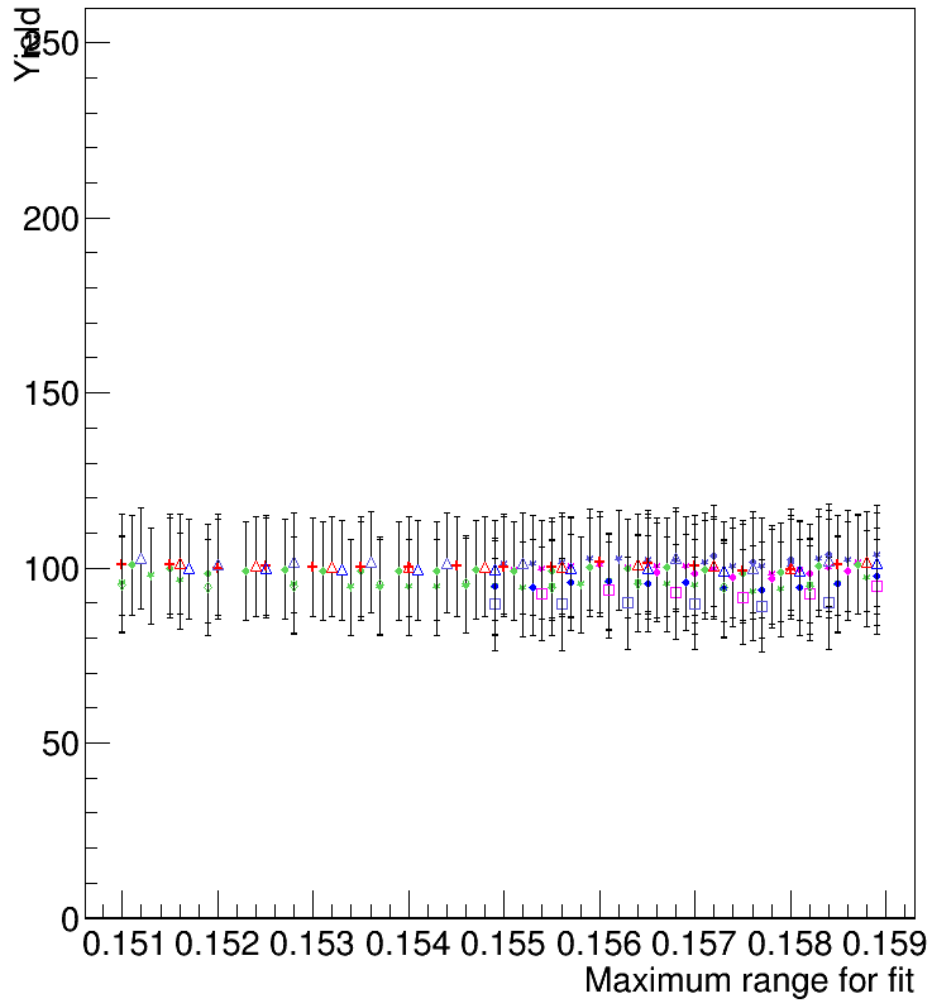


Figure 17: The yields given by fits as a function of the maximum range, points with the same color have the same first used bin, points with the same marker have the same rebinvalue.

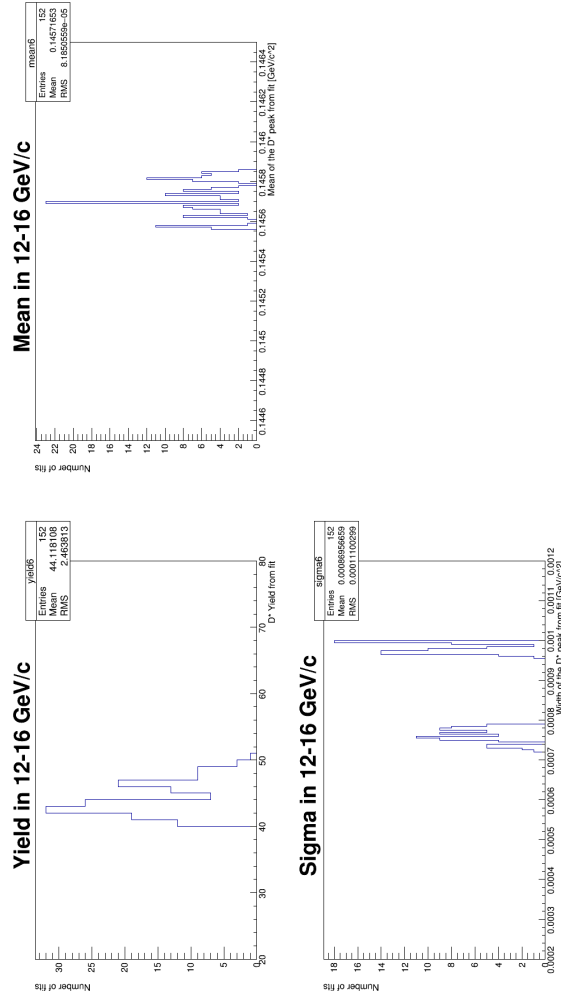


Figure 18: The yield, mean and sigma for the 12-16 GeV pt-bin.

yield 12-16 GeV/c

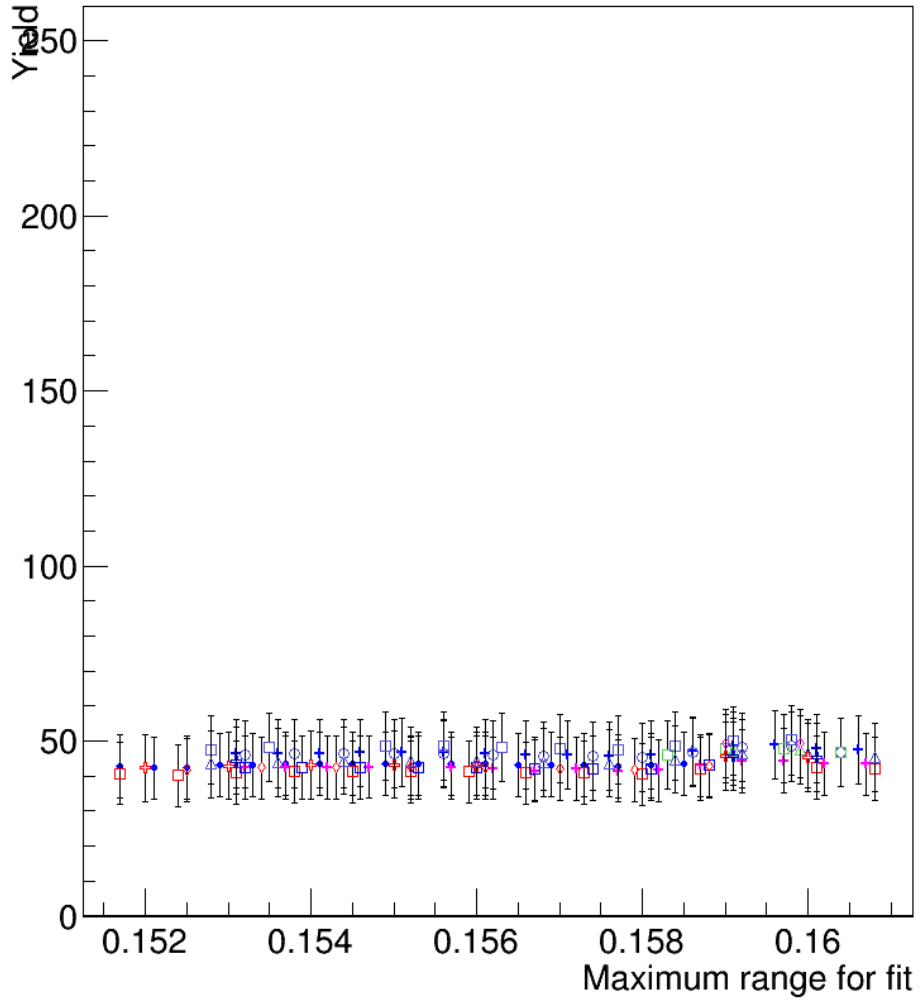


Figure 19: The yields given by fits as a function of the maximum range, points with the same color have the same first used bin, points with the same marker have the same rebinvalue.

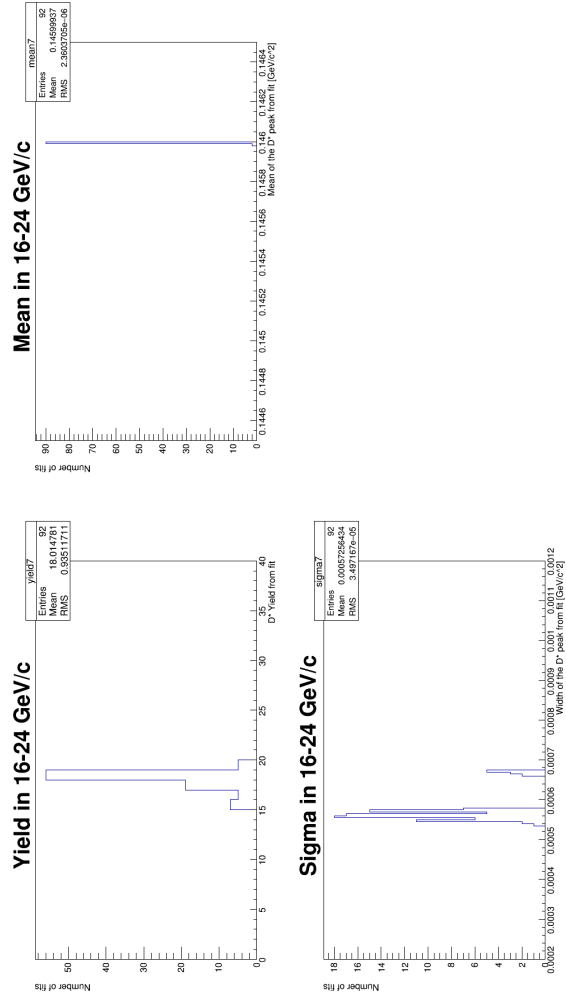


Figure 20: The yield, mean and sigma for the 16-24 GeV pt-bin.

yield 16-24 GeV/c

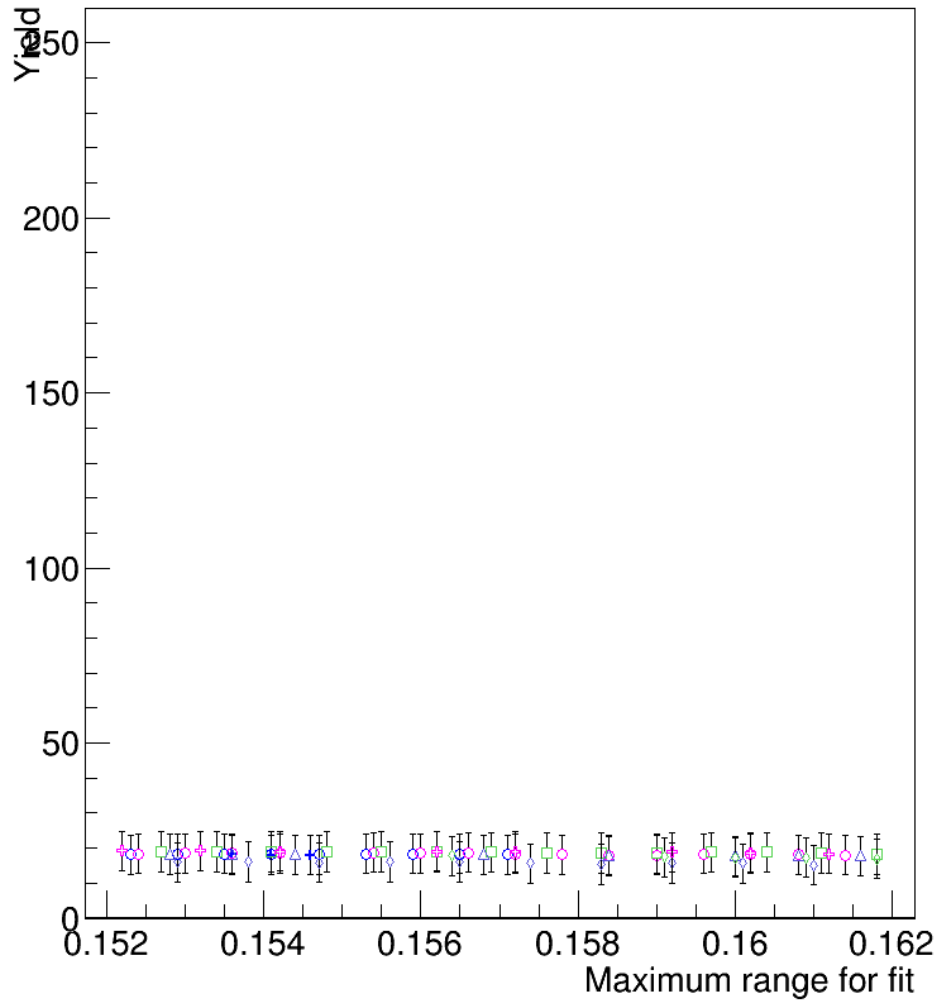


Figure 21: The yields given by fits as a function of the maximum range, points with the same color have the same first used bin, points with the same marker have the same rebinvalue.

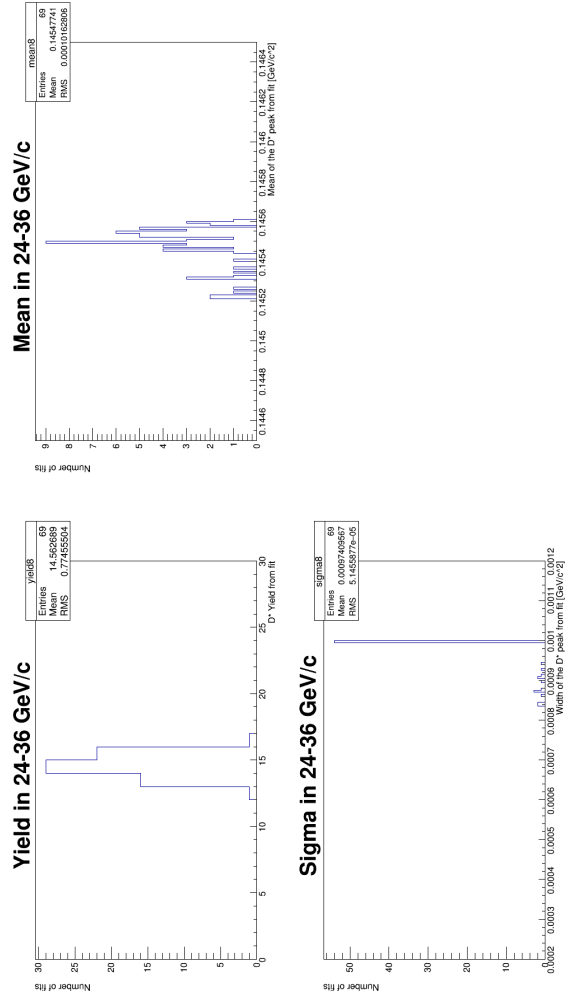


Figure 22: The yield, mean and sigma for the 24-36 GeV pt-bin.

yield 24-36 GeV/c

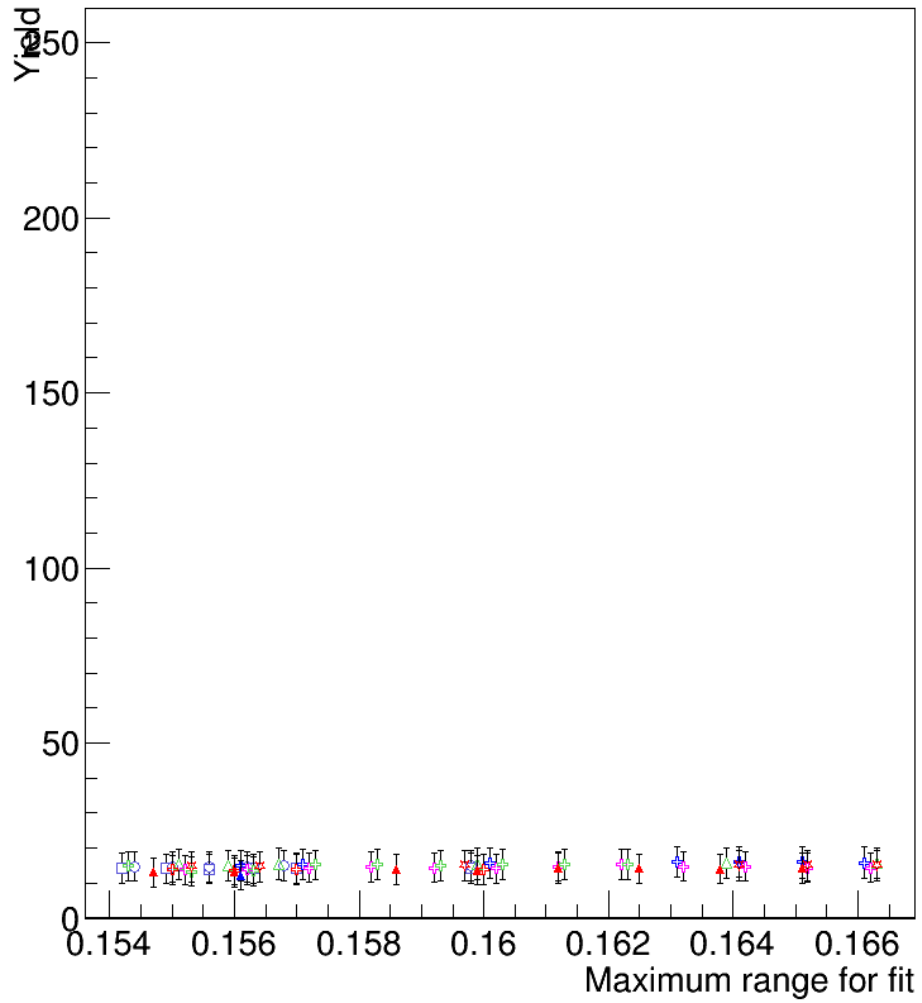


Figure 23: The yields given by fits as a function of the maximum range, points with the same color have the same first used bin, points with the same marker have the same rebinvalue.